and tail winds. They argued that these differences could be explained by wing loading per aspect ratio and wing root thickness. The series solution shows that the optimum glide velocity in a head wind or tail wind depends only on the wind velocity and the zero-wind optimum glide velocity. Therefore, gliders with parabolic drag polars having identical zero-wind optimum glide velocities will have identical optimum velocities in a head wind or tail wind, despite having different geometric shapes and wing loading.

Conclusion

An alternative solution of the optimum gliding speed in a steady head wind or tail wind has been found. This equation solves the gliding velocity in terms of the zero-wind glide velocity and the wind velocity, and it clearly shows that the optimum glide velocity is solely determined by these two variables. The solution is valid for wind speeds up to the zero-wind optimum glide velocity and requires no curve fitting or coefficient calculations. The solution also demonstrates mathematically why a head wind will always require a greater velocity correction than a tail wind for optimum gliding flight.

Acknowledgments

The author would like to thank the reviewer for the helpful comments and criticisms that resulted in defining the region of convergence for the series solution. Acknowledgment is also given to the readers of the bulletin board "rec.aviation" who asked the question about optimum glide speed in a head wind or tail wind.

References

[1]MacCready, P. B., "Optimum Airspeed Selector," *Soaring*, Vol. 18, No. 2, 1954, pp. 16–21.

[2]MacCready, P. B., "Understanding Speed-to-Fly and the Speed Ring," *Soaring*, Vol. 47, No. 5, 1982, pp. 42–47.

[3]Kuettner, J. P., "The 2000 Kilometer Wave Flight—Part II," *Soaring*, Vol. 49, No. 3, 1985, pp. 22–27.

[4]Reichmann, H., *Cross-Country Soaring*, Thomson, Pacific Palisades, CA, 1978, p. 98.

[5]Jenkins, S. A., and Wasyl, J., "Optimization of Glides for Constant Wind Fields and Course Headings," *Journal of Aircraft*, Vol. 27, No. 7, pp. 632–638.

[6]Shevell, R. S., *Fundamentals of Flight*, 2nd ed., Prentice-Hall, Englewood Cliffs, NJ, p. 185.

[7]Burrington, R. S., *Handbook of Mathematical Tables and Formulas*, 4th ed., McGraw-Hill, New York, p. 13.

[8]Soaring Society of America, *Soaring Flight Manual*, Jeppesen Sanderson, Inc., Englewood, CO, 1980, Chap. 2, p. 7.

[9]Miele, A., *Flight Mechanics—Theory of Flight Paths, Vol. 1*, Addison-Wesley, Reading, MA, 1962, p. 153.

[10]Jenkins, S. A., Armi, L., and Wasyl, J., "Glide Optimization for Cross Country Wave Flights," *Technical Soaring*, Vol. 16, No. 1, 1992, pp. 3–16.

Navier-Stokes Investigation of Blunt Trailing-Edge Airfoils Using O Grids

M. Khalid* and D. J. Jones†
Institute for Aerospace Research, National Research Council of Canada, Ottawa, Ontario K1A 0R6, Canada

Received June 25, 1992; revision received Nov. 2, 1992; accepted for publication Nov. 13, 1992.

*Associate Research Officer, High Speed Aerodynamics Laboratory.

†Senior Research Officer, High Speed Aerodynamics Laboratory. Member AIAA.

Introduction

SOME recent papers[1-3] have investigated the flowfield past a blunt trailing-edge airfoil. We show here that the standard ARC2D[4] code (Baldwin-Lomax) can be used for blunt trailing-edge airfoils with the computational domain configured as an O-grid, rather than using a complex C-H-grid,[1] requiring higher order turbulence models for convergence. See Ref. 5 for details.

Four airfoils 1) RAE2822 (1.12%), 2) FIN5LLT1 (0.7%), 3) FINLLT2 (1.49%), and 4) WTEA (0.5%) were investigated. The percentages in brackets refer to the trailing-edge thickness with respect to the chord. The O-grids around the airfoils were generated using an algebraic generator ALGGRID.[5] A typical O-grid around a blunt trailing-edge airfoil is shown in Fig. 1.

Results and Discussion

Figures 2 and 3 show the pressure coefficient comparisons with measured data for cases 1 and 2 for the RAE2822 airfoil. The agreement between the measured data (taken directly from Ref. 1) and computations for case 2 is quite good. For case 1, except for a small portion close to the leading edge on the upper surface, the pressures are well matched. The agreement for the lower surface, however, is not as good, especially in the forward regions.

The comparison of the coefficient of pressure with measured data, in the range $0.86 < x/c < 1.0$, for cases 1 and 2 are shown in Figs. 4 and 5, respectively. In this particular exercise the Navier-Stokes code was run with both the Baldwin-Lomax model as well as a mixing length turbulence model. The other results shown in the figures (taken from Ref. 1),

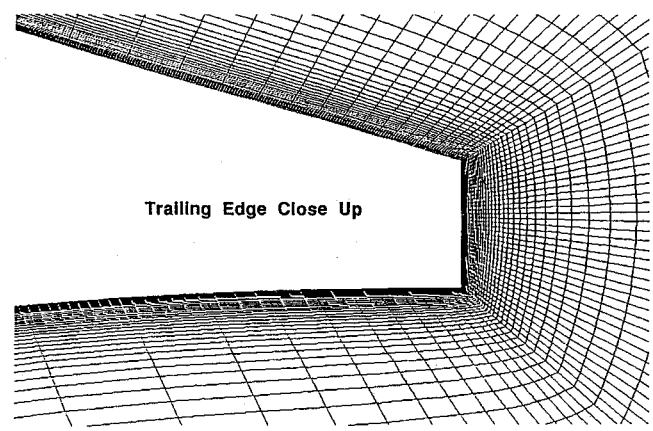

Fig. 1 Structured "O" grid around the blunt trailing-edge airfoil FIN5LLT2.

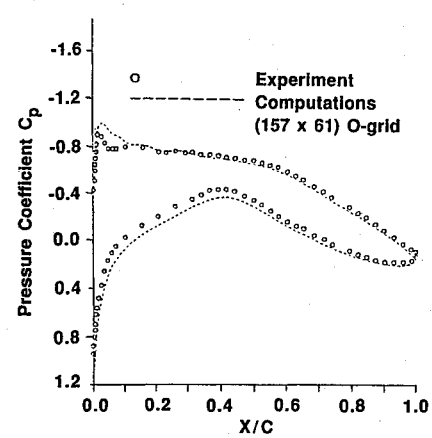

Fig. 2 Comparison of computed and measured data on blunt RAE2822 airfoil for case 1, $M_\infty = 0.676$, $\alpha = 2.45$, $Re = 5.4 \times 10^6$. Transition at $x/c = 0.11$ for upper and lower surfaces.

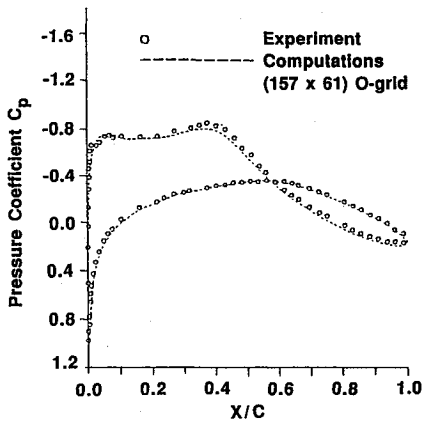

Fig. 3 Comparison of computed and measured data on blunt RAE2822 airfoil for case 2, $M_\infty = 0.676$, $\alpha = -2.06$, $Re = 5.4 \times 10^6$. Transition at $x/c = 0.11$, upper and lower surfaces.

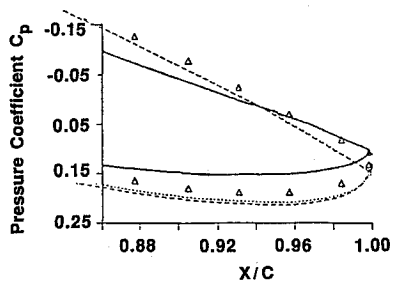

Fig. 4 Comparison of data close to the trailing edge (case 1). Δ, Experiment; ----- mixing length turbulence model (present); ····· Baldwin-Lomax (present); —·—·—· Spalart turbulence model (1); ——— Baldwin-Barth turbulence model (1).

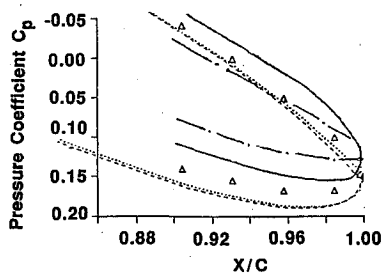

Fig. 5 Comparison of data close to the trailing edge (case 2). Δ, Experiment; ----- mixing length turbulence model (present); ····· Baldwin-Lomax (present); —·—·—· Spalart turbulence model (1); ——— Baldwin-Barth turbulence model (1).

use a one-equation turbulence model on a C-H-grid. As expected, the Baldwin-Lomax and mixing length turbulence models give very similar results. It appears that the results from present computations are as good as, if not better than, the results obtained from the one-equation turbulence models due to Baldwin-Barth[1] and Spalart-Allmaras.[1]

Pressure coefficient contours close to the trailing edge are shown in Fig. 6. In terms of absolute values, the present computations and the ones obtained using Baldwin-Barth turbulence model[1] come closest to the measured values.

The velocity profiles for case 1 at axial stations of $x/c = 0.96$ and $x/c = 1.0$ are shown in Figs. 7 and 8. At $x/c = 0.96$, on the upper surface, the present computations are as well matched as the other two reported in Ref. 2. For the lower surface, however, the comparison for most parts is much better than the results reported for the Baldwin-Barth and Spalart-Allmaras turbulence models.[1] Near the edge of the boundary layer, on the other hand, present computations show a slower growth of the boundary layer. Increasing the number of grid lines within the boundary layer made no difference to

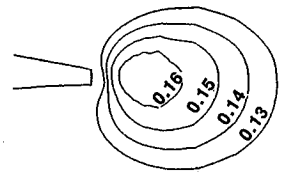

a) Spalart-Allmaras model

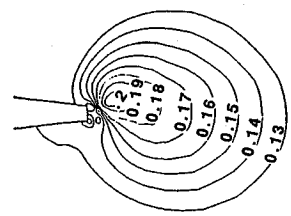

b) Baldwin-Barth model

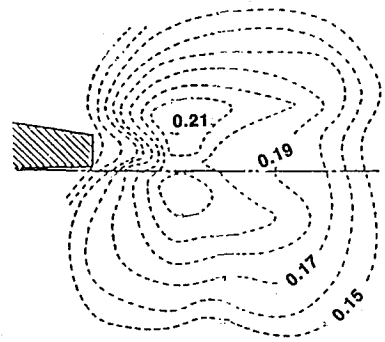

c) Experiment Ref. 1

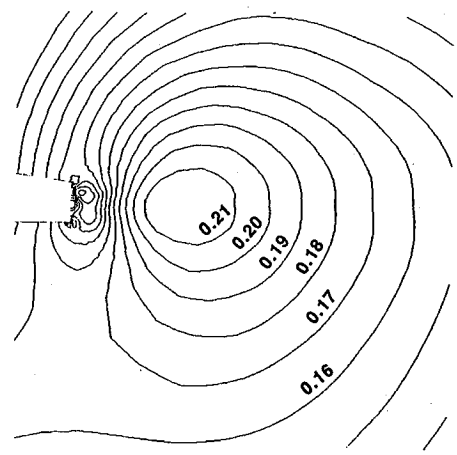

d) Present computations (case 1)

Fig. 6 Pressure coefficient contours in the trailing-edge region for a) and b) the one-equation turbulence models, c) the experiment Ref. 1, and d) case 1.

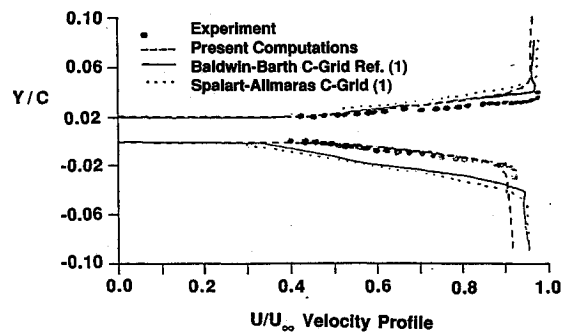

Fig. 7 Comparison of velocity profiles at $x/c = 0.96$.

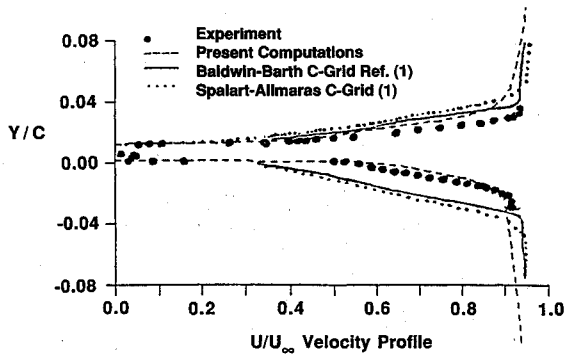

Fig. 8 Comparison of velocity profiles at $x/c = 1.0$.

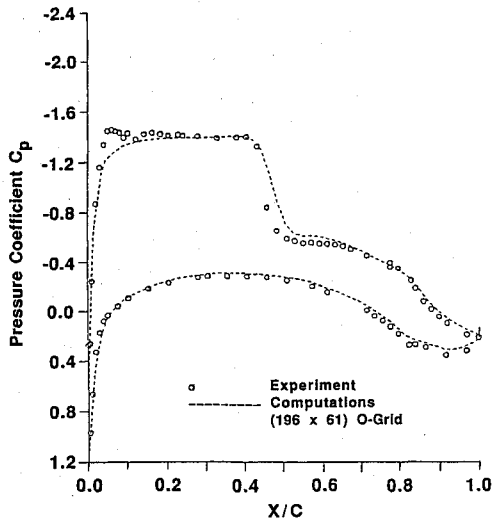

Fig. 9 Comparison of computed and measured data on blunt FIN5LLT1 airfoil for $M_\infty = 0.72$, $C_L = 0.73$, $Re_c = 14 \times 10^6$. Transition, upper surface $x/c = 0.07$; lower surface $x/c = 0.15$.

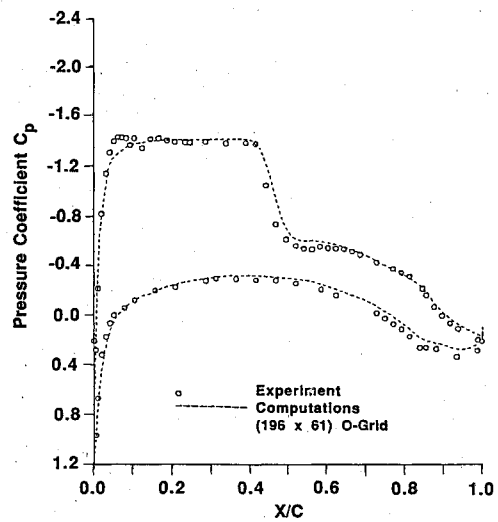

Fig. 10 Comparison of computed and measured data on blunt FIN5LLT2 airfoil for $M_\infty = 0.72$, $C_L = 0.707$, $Re_c = 14 \times 10^6$. Transition, upper surface $x/c = 0.15$; lower surface $x/c = 0.07$.

the results. The comparison at $x/c = 1$ is as good as at the earlier station, $x/c = 0.96$.

C_P comparisons against measured data are shown in Figs. 9 and 10 for FIN5LLT1 and FIN5LLT2, respectively. Note that while no Mach number corrections were applied to the experimental data, an approximate angle-of-attack correction was implemented. The computations were therefore carried out at $M_\infty = 0.7$ instead of the tunnel value of $M_\infty = 0.72$ to account for the floor, ceiling as well as a small sidewall correction. The correction methods are referenced in Ref. 5. The iterations during computation proceeded until the computed lift coefficient converged to the tunnel lift coefficient. Except for a small region close to the leading edge on the upper surface where computations overpredict the pressures, a reasonable agreement between measured and computed values is obtained.

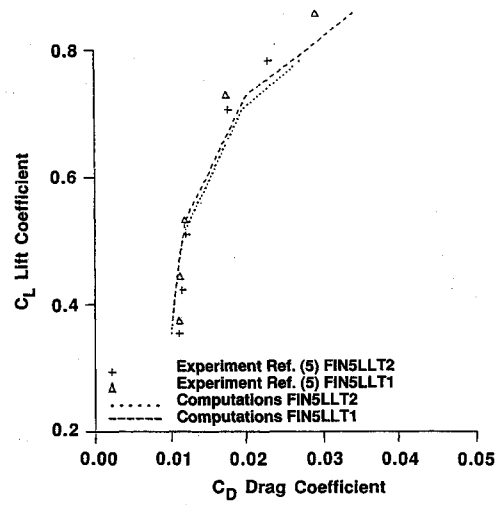

Fig. 11 Drag polars at $M_\infty = 0.72$, $Re_c = 14 \times 10^6$ for FIN5LLT1 and FIN5LLT2.

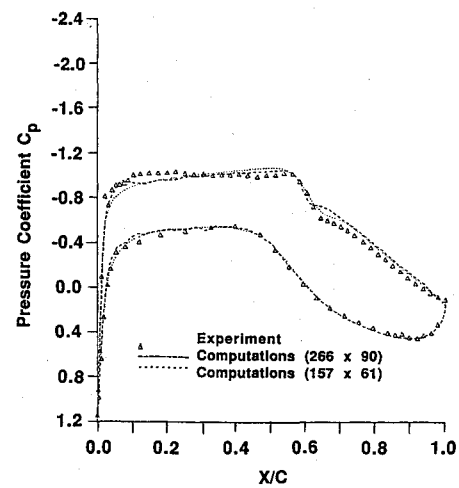

Fig. 12 Comparison of computed and measured data on blunt trailing-edge airfoil WTEA. $M_\infty = 0.748$, $C_L = 0.60$, $Re_c = 8 \times 10^6$. Transition, at $x/c = 0.08$, upper and lower surfaces.

The measured and computed drag polars for a set of five C_L and α values are shown in Fig. 11. The flow conditions for the drag polars were $M_\infty = 0.72$ and $Re/c = 14 \times 10^6$. It is quite apparent that for small angles of attack, where the flow is mostly attached, the computed drag for both airfoils compares quite favorably with the experiment.

The pressure comparison for the 16% thick natural laminar flow airfoil WTEA is shown in Fig. 12. The experimental results already contained the tunnel floor and ceiling correction, however, an estimated sidewall correction of $\Delta M = 0.023$, was applied prior to the Navier-Stokes computations. For comparison sake, the results from a finer grid (266 × 90) obtained from a hyperbolic grid generation package are also shown along with the results from a coarser local grid (157 × 61) generated from ALGGRID. The coarse grid performed as well as the finer grid, while the convergence time for the finer grid was roughly twice that of the coarse one. The agreement between theory and experiment for this 16% thick natural laminar flow (NLF) airfoil is as good as seen in the earlier cases.

Conclusion

Although the Baldwin-Lomax turbulence model may not, in principle, be well-suited for the wake region immediately behind the trailing-edge, it has been shown that accurate results can be obtained using this model on O-grid-based airfoil meshes.

Acknowledgments

The authors thank T. Pulliam (NASA Ames) for releasing the ARC2D program to the Institute for Aerospace Research. They also thank I. Fejtek (deHavilland) for providing the finer grid used for comparison in Fig. 12.

References

[1]Stanaway, S. K., McCrosky, W. J., and Kroo, I. M., "Navier-Stokes Analysis of Blunt Trailing Edge Airfoil," AIAA Paper 92-0024, Jan. 1992.

[2]Chan., J. S., "Multizone Navier-Stokes Computations of Viscous Transonic Flows Around Airfoils," AIAA Paper 88-0103, Jan. 1988.

[3]Drela, M., "Integral Boundary Layer Formulation for Blunt Trailing Edges," AIAA Paper 89-2166-CP, July 1989.

[4]Pulliam, T., "Euler and Thin Layer Navier-Stokes Codes: ARC2D and ARC3D," Notes for Computational Fluid Dynamics User's-Workshop UTSI E02-4005-023-84, March 1984.

[5]Khalid, M., and Jones, D. J. "A Study of Blunt Trailing Edge Airfoils Using the Navier Stokes Code—ARC2D," Canadian Aeronautics and Space Inst. Conf., Toronto, May 1993 (to be published).